Characteristic scales of Townsend's wall-attached eddies

By A. Lozano-Durán AND H. J. Bae

1. Motivation and objectives

At first sight, walls appear as the most relevant constituent of turbulence confined or limited by solid surfaces, and it seems natural to assume that they should be the source and organizing agent of wall-bounded turbulence. Consequently, many efforts have been devoted to understanding the structure of turbulence in the presence of walls. Particularly interesting is the region within the so-called logarithmic layer (log-layer), where most of the dissipation resides in the asymptotic limit of infinite Reynolds number (Marusic *et al.* 2013). The seminal work by Townsend (1976) conceived the flow across the log-layer as a self-similar population of eddies of different sizes attached to the wall and organized according to the only meaningful physical quantities once viscosity is dismissed, i.e., the friction velocity and the distance to the wall. In the present work, we propose an extension of Townsend's model for the momentum-carrying log-layer motions, where the length and velocity scales of the eddies are controlled by the turbulent energy production rate with no direct reference to the distance to the wall.

In addition to Townsend's attached eddy model (Townsend 1976) and subsequent refinements by Perry & Chong (1982) and Meneveau & Marusic (2013) (see Marusic & Monty 2019, for a comprehensive review), the presence of walls is key for many low-order models and theories aiming to understand the outer-layer dynamics. In the hairpin packet model (Adrian *et al.* 2000), arch-like eddies are created at the wall and migrate away from it. Alternative models by Davidson *et al.* (2006) do not require wall-attached eddies but still rely on the distance to the wall as a fundamental scaling property of the flow. The aforementioned proportionality of the sizes of eddies with the wall-normal distance was originally hypothesized as an asymptotic limit at very high Reynolds numbers and used in the classical derivation of the logarithmic velocity profile (Millikan 1938), but it has been observed experimentally and numerically in spectra and correlations at relatively modest Reynolds numbers in pipes (Morrison & Kronauer 1969; Perry & Abell 1977; Bullock *et al.* 1978; Kim & Adrian 1999; Guala *et al.* 2006; Bailey *et al.* 2008) and in turbulent channels and flat-plate boundary layers (Tomkins & Adrian 2003; del Álamo *et al.* 2004; Monty *et al.* 2007; Hoyas & Jiménez 2008). In this framework, the mechanism by which eddies can "feel" the distance to the wall is through the no transpiration boundary condition or impermeability.

Previous studies have also revealed that the outer flow can survive independently of the particular configuration of the eddies closest to the wall. The most well-known examples are the roughness experiments where properties of the logarithmic and outer layers remain essentially unaltered despite the fact that roughness destroys the near-wall region (Perry & Abell 1977; Jiménez 2004; Bakken *et al.* 2005; Flores *et al.* 2007). The independence of the outer layer with respect to the details of the near-wall region was formulated by Townsend (1976) in the context of rough walls, and it is usually referred to as Townsend's similarity hypothesis. The numerical study by Chung *et al.* (2014)

assessed an idealized version of the Townsend's similarity hypothesis by introducing slip velocities parallel to the wall while still invoking the no transpiration condition for the wall-normal velocity. Flores & Jiménez (2006) showed that the characteristics of the outer part of a channel flow remain unchanged when perturbing the velocities at the wall. Although transpiration at the wall was allowed, it was only for a selected set of wavenumbers and the wall was still perceived as impermeable by most of the flow scales. Mizuno & Jiménez (2013) performed computations of turbulent channels in which the wall was substituted by an off-wall boundary condition mimicking the expected behavior from an extended logarithmic layer (and hence, a wall), bypassing the buffer layer, with relatively few deleterious effects on the flow far from the boundaries.

In the present work, we propose characteristic velocity, length, and time scales of the momentum-carrying eddies by assuming that they are exclusively controlled by the mean momentum flux and mean shear without explicit reference to the wall.

The brief is organized as follows. The new characteristic scales are presented in Section 2. The proposed scaling is assessed in turbulent channel flows with modified mean momentum flux in Section 3. In Section 4, we introduce turbulent channels where the no-slip walls are replaced by Robin boundary conditions for the three velocity components to analyze the effect of the impermeability condition. Concluding remarks are finally made in Section 5.

2. Scales controlling wall-attached eddies

We consider a statistically steady, wall-bounded turbulent flow confined between two parallel walls where u_i with $i = 1, 2, 3$ are the streamwise, wall-normal, and spanwise velocities, respectively. The pressure is denoted by p. The three spatial directions are x_i with $i = 1, 2, 3$, and the walls are located at $x_2 = 0$ and $x_2 = 2h$ where h is the channel half-height. The fluid is incompressible with kinematic viscosity ν. We further assume that the flow is homogeneous in the streamwise and spanwise directions.

First, we briefly revisit the classic scaling by Townsend (1976). The traditional argument for the characteristic velocity of eddies transporting tangential Reynolds stress is that their associated turbulence intensities equilibrate to comply with the mean integrated momentum balance

$$\langle u_1 u_2 \rangle \approx u_\tau^2 \left(\frac{x_2}{h} - 1 \right), \tag{2.1}$$

where the viscous effects have been neglected, $\langle \cdot \rangle$ denotes averaging in the homogeneous directions and time, and $u_\tau = \sqrt{\nu \partial \langle u_1 \rangle / \partial x_2}$ is the so-called friction velocity. Hence, the relevant velocity scale at all wall-normal distances is identified as u_τ. Regarding the characteristic length scale, the classic theory states that the log-layer motions are too large to be affected by viscosity but small compared to the most restrictive boundary layer limit $\mathcal{O}(h)$. It is argued then that the most meaningful length scale the log-layer eddies can be influenced by is the distance to the wall.

The hypothesis under consideration here is that the wall is not the organizing element of the momentum-carrying eddies, whose intensities and sizes are controlled instead by the mean production rate of turbulent kinetic energy, i.e., by the mean momentum flux $-\langle u_1 u_2 \rangle$ and associated mean shear $\partial \langle u_1 \rangle / \partial x_2$. The proposed characteristic length l^*, time t^*, and velocity u^* scales of wall-attached eddies are sketched in Figure 1.

The characteristic velocity promoted in the present work is dictated by the momentum flux $u^* \sim \sqrt{-\langle u_1 u_2 \rangle}$. For comparisons with the classic scaling by u_τ, we define a new

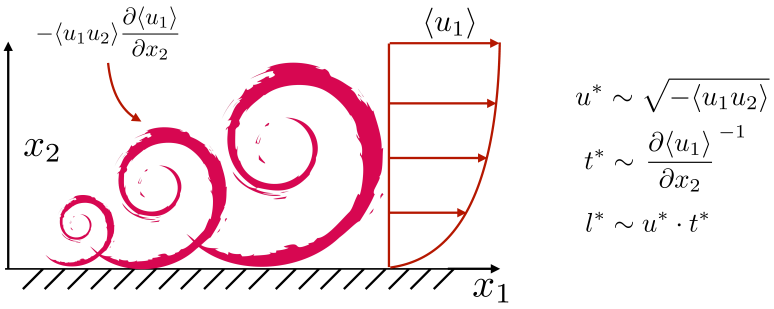

FIGURE 1. Sketch of wall-attached momentum-carrying eddies of different sizes in a turbulent boundary layer controlled by the mean production rate of turbulent kinetic energy, $-\langle u_1u_2\rangle\partial\langle u_1\rangle/\partial x_2$, and proposed velocity, time and length scales.

characteristic velocity by analogy with Eq. (2.1) (Tuerke & Jiménez 2013) as

$$u^* \equiv \sqrt{\frac{-\langle u_1u_2\rangle}{1-x_2/h}}. \tag{2.2}$$

Note that we could have also used $u^* \equiv \sqrt{-\langle u_1u_2\rangle}$, and the wall-normal coordinate x_2/h contained in the left-hand side of Eq. (2.2) is not a definitory element of u^*. The factor $\sqrt{1-x_2/h}$ is introduced in Eq. (2.2) only for convenience such that u^* collapses to u_τ for a channel flow driven by a constant pressure gradient.

The scenario proposed for the characteristic time and length scales of wall-attached eddies also differs from the classic theory. Let us consider a momentum-carrying eddy of size $l^* \sim u^* \cdot t^*$ controlled by the injection of energy from the mean shear and, therefore, with characteristic lifespan

$$t^* \equiv \left(\frac{\partial\langle u_1\rangle}{\partial x_2}\right)^{-1}. \tag{2.3}$$

The scaling in Eq. (2.3) can also be interpreted as the average time for the eddies to extract energy from the mean shear. Considering the scaling suggested for u^* in Eq. (2.2), the resulting length scale is

$$l^* \equiv u^* \cdot t^* = \sqrt{\frac{-\langle u_1u_2\rangle}{1-x_2/h}}\left(\frac{\partial\langle u_1\rangle}{\partial x_2}\right)^{-1}. \tag{2.4}$$

Equation (2.4) can also be obtained by assuming that the momentum-carrying eddies are controlled by the mean production rate of turbulent kinetic energy, $P = -\langle u_1u_2\rangle\partial\langle u_1\rangle/\partial x_2 \sim u^{*3}/l^*$, which together with Eq. (2.2) yields an expression identical to Eq. (2.4).

For the particular case of a plane channel flow with no-slip walls and constant mean pressure gradient, we recover $u^* = u_\tau$. Moreover, the characteristic length l^* in the log-region of the flow with mean shear $\partial\langle u_1\rangle/\partial x_2 = u_\tau/(\kappa x_2)$ reduces to

$$l^* = u_\tau\left(\frac{\partial\langle u_1\rangle}{\partial x_2}\right)^{-1} \approx \kappa x_2, \tag{2.5}$$

which is proportional to the distance to the wall as commonly discussed in the literature. Therefore, the extension of the characteristic scales proposed above collapses to

Townsend's model for a canonical case. It is important to remark that despite the fact that the velocity and length scales specified by u^* and l^* coincide with their classic counterparts u_τ and x_2 for the traditional channel flow, the former are conceptually distinct as they remain agnostic to the location of the wall.

3. Turbulent channel with modified mean pressure gradient

3.1. *Numerical scheme and computational domain*

We perform a set of direct numerical simulations (DNS) of plane turbulent channel flows by solving the incompressible Navier-Stokes equations with a staggered second-order finite difference (Orlandi 2000) and a fractional-step method (Kim & Moin 1985) with a third-order Runge-Kutta time-advancing scheme (Wray 1990). Periodic boundary conditions are imposed in the streamwise and spanwise directions, and no-slip at the walls. The code has been validated in previous studies in turbulent channel flows (Lozano-Durán & Bae 2016; Bae *et al.* 2018*a*,*b*) and flat-plate boundary layers (Lozano-Durán *et al.* 2018).

Wall units are denoted by the superscript + and defined in terms of the kinematic viscosity ν and friction velocity at the wall u_τ. Accordingly, the friction Reynolds number is $Re_\tau = u_\tau h/\nu$. Velocities normalized by u^* are denoted by the superscript $*$. Fluctuating quantities with respect to the mean are represented by $(\cdot)'$.

3.2. *Numerical experiments of channels with modified mean pressure gradient*

We devise two sets of conceptual numerical experiments to unravel the characteristic scales of the outer-layer motions. The first set of experiments is a channel flow with no-slip walls and modified x_2-dependent mean pressure gradients of the form

$$\left\langle \frac{\mathrm{d}p}{\mathrm{d}x_1} \right\rangle = -\frac{u_\tau^2}{h}\left[1 + \epsilon\left(2x_2/h - x_2^2/h^2\right) - 2/3\epsilon\right], \tag{3.1}$$

where ϵ is a non-dimensional adjustable parameter. Equation (3.1) is such that Re_τ remains unchanged with ϵ. The goal is to alter the natural balance between eddies which are forced to readjust their intensities to accommodate the new momentum flux. Two cases are considered: $\epsilon = 4$, labeled as NS550-p, and $\epsilon = -2$, labeled as NS550-n, where NS denotes no-slip.

The second set of experiments intends to clarify the characteristic length scales of the active energy-containing eddies. The change in u^* and t^* from NS550-p and NS550-n is not significant enough to assess conclusively the scaling proposed in Eq. (2.4). For that reason, two new simulations, NS550-s1 and NS550-s2, are considered by prescribing a synthetic mean velocity profile of the form

$$\frac{\langle u_1 \rangle}{u_{\mathrm{ref}}} = \frac{\alpha+2}{\alpha+1}\left[1 - (x_2/h - 1)^{\alpha+1}\right] + \frac{\beta+2}{\beta+1}\left[1 - (x_2/h-1)^{\beta+1}\right], \tag{3.2}$$

with $(\alpha, \beta) = (41, 11)$ and $(3, 3)$ for NS550-s1 and NS550-s2, respectively. The parameter u_{ref} was adjusted to achieve $Re_\tau \approx 550$. The profiles from Eq. (3.2) are purposely tailored to create distinguishable l^* with values equal to $0.06h$, $0.03h$, and $0.04h$ at $x_2 = 0.10h$, for cases NS550, NS550-s1, and NS550-s2, respectively. All the cases above are designed such that u_τ and x_2 remain unchanged but do not coincide with the scaling proposed by u^* and l^*, in contrast to the traditional channel flow, where $u^* \approx u_\tau$ and $l^* \approx \kappa x_2$. This will allow us to assess the validity of each scaling.

Case	Re_τ	Δx_1^+	$\Delta x_{2,min/max}^+$	Δx_3^+	Driven by
NS550-p	546	6.7	0.2/9.9	3.3	modified $\langle \frac{\mathrm{d}p}{\mathrm{d}x_1} \rangle$
NS550-n	546	6.7	0.2/9.9	3.3	modified $\langle \frac{\mathrm{d}p}{\mathrm{d}x_1} \rangle$
NS550-s1	531	6.5	0.2/9.7	3.2	prescribed $\langle u_1 \rangle$
NS550-s2	546	6.7	0.2/9.9	3.3	prescribed $\langle u_1 \rangle$

TABLE 1. Tabulated list of cases. The numerical experiments are labeled following the convention NS[Re_τ]-[specific case], where NS denotes channel with no-slip walls. Δx_1, Δx_2 and Δx_3 are the streamwise, wall-normal, and spanwise grid resolutions, respectively. The last column shows the method employed to drive the channel flow. See text for details.

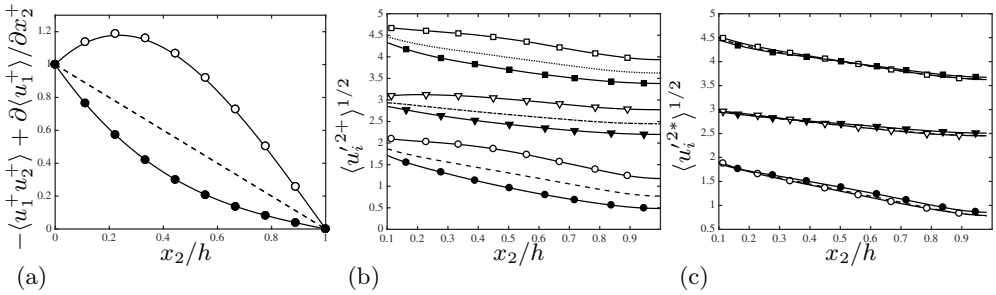

FIGURE 2. Mean (a) total tangential Reynolds stress for NS550 (dashed line), NS550-p (open circles), and NS550-n (closed circles). Panels (c) and (d) contain the streamwise (circles), wall-normal (triangles), and spanwise (squares) root-mean-squared velocity fluctuations scaled with (c) u_τ and (d) u^*. Open and closed symbols for R550-p and R550-n, respectively.

The list of cases is summarized in Table 1. All the simulations were run for at least 10 eddy turnover times (defined as h/u_τ) after transients. We compare our results with DNS data from del Álamo & Jiménez (2003) and Hoyas & Jiménez (2006) at $Re_\tau \approx 550, 950,$ and 2000, which are labeled as NS550, NS950, and NS2000, respectively.

3.3. *Assessment of characteristic velocity and length scales*

We examine scaling from Eq. (2.2) in turbulent channel flows with modified mean pressure gradients given by Eq. (3.1). The imposed x_2-dependent pressure gradient breaks the global velocity scale with u_τ, and the new balance for the mean momentum flux requires that $\langle u_1 u_2 \rangle \approx \int_0^{x_2} - \langle \mathrm{d}p/\mathrm{d}x_1 \rangle \, \mathrm{d}x_2$. The total stresses consistent this new set-up for cases NS550-p and NS550-n are shown in Figure 2(a).

The three root-mean-squared (r.m.s.) fluctuating velocities for NS550, NS550-p, and NS550-n are reported in Figure 2(b). The pronounced lack of collapse among the three cases exposes the unsatisfactory scaling with u_τ. Conversely, when the r.m.s. fluctuating velocities are scaled with u^*, which can be analytically evaluated for cases NS550-p and NS550-n, the agreement is excellent (Figure 2c). Note that the argument above holds for Townsend's active motions, i.e., those responsible for the mean momentum transfer, and that the inactive motions are not expected to scale with u^* but with the bulk velocity or

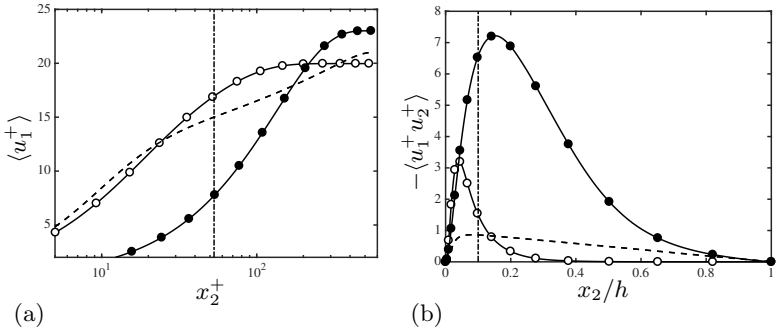

FIGURE 3. Mean (a) streamwise velocity profile and (b) tangential Reynolds stress. Lines and symbols are: dashed line for NS550, open circles for NS550-s1, and closed circles for NS550-s2. The dash-dotted line is $x_2 = 0.1h$.

a mixed scale as suggested in previous works (De Graaff & Eaton 2000; del Álamo *et al.* 2004; Vallikivi *et al.* 2015).

Scaling from Eq. (2.4) is investigated in cases NS550, NS550-s1, and NS550-s2 with mean velocity profiles shown in Figure 3(a). Figure 3(b) contains the tangential Reynolds stress artificially generated to sustain $\langle u_1 \rangle$. The relevant length scale of the momentum-carrying eddies is examined in Figure 4 by comparing the premultiplied, two-dimensional velocity spectra at $x_2 = 0.10h$ as a function of the streamwise and spanwise wavelengths (λ_1 and λ_3) scaled by the distance to the wall (top panels) and l^* (bottom panels). The spectra display a noticeable mismatch when the wavelengths are scaled by x_2, whereas the collapse is appreciably improved when λ_1 and λ_3 are normalized by l^*, especially for the most intense spectral cores. Therefore, l^* stands as a more faithful characterization of the eddy sizes compared to the distance to the wall.

In summary, we have shown that u^* and l^* are tenable candidates to represent the characteristic scales of the momentum-carrying eddies in wall-bounded turbulence. The proposed scales are still consistent with the classic scaling provided by u_τ and x_2, and can be considered as an extension for more general shear-dominated turbulence.

4. Turbulent channel with Robin boundary conditions

In this section, we analyze the significance of the distance to the wall for the outer flow by using turbulent channel flows where the no-slip wall is replaced by Robin boundary conditions. The new set-up allows for instantaneous velocities at the boundaries and, in particular, for wall-normal transpiration. No transpiration is considered to be the most distinctive feature of walls, and it is commonly understood as the mean by which the log-layer motions "feel" the distance to the wall. Hence, the non-zero u_2 at $x_2 = 0$ (and $x_2 = 2h$) introduced by the Robin boundary condition is intended to assess the role of impermeable walls as organizing agents of wall-attached eddies.

4.1. *Numerical experiments of channels with Robin boundary conditions*

We perform a set of DNS of turbulent channel flows using the same numerical scheme and computational domain discussed in Section 3.1. The effect of a permeable boundary is investigated by replacing the traditional no-slip boundary condition by a Robin boundary

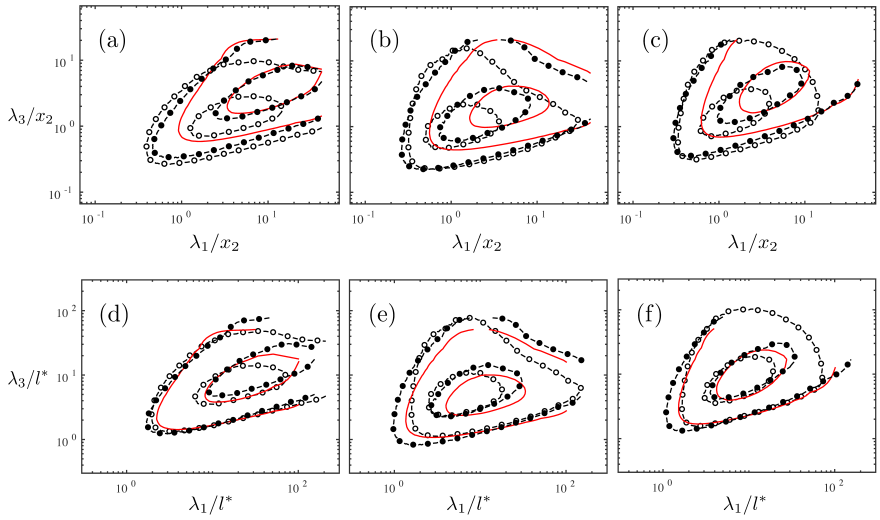

FIGURE 4. Premultiplied streamwise (a,d), wall-normal (b,e), and spanwise (c,f) velocity spectra at $x_2 = 0.10h$ for NS550 (solid red), NS550-s1 (open circles), and NS550-s2 (closed circles). The wavelengths are scaled by x_2 for the top panels and by l^* for the bottom panels. Contours are 0.1 and 0.6 of the maximum.

condition of the form

$$u_i|_w = l \left. \frac{\partial u_i}{\partial n} \right|_w, \quad i = 1, 2, 3, \tag{4.1}$$

where the subscript w refers to quantities evaluated at the wall, and n is the wall-normal (or boundary-normal) direction. We define l to be the slip length that, in general, may be a function of the spatial wall-parallel coordinates and time. The choice of l must comply with the symmetries of the flow and, particularly for a channel flow configuration, Eq. (4.1) should satisfy

$$\langle u_i|_w \rangle = \left\langle l \left. \frac{\partial u_i}{\partial x_2} \right|_w \right\rangle = 0, \quad i = 2, 3. \tag{4.2}$$

In the present study, we consider a constant value for l. This is consistent with Eq. (4.2) because $\langle u_i|_w \rangle = 0$ and $\langle \partial u_i/\partial x_2|_w \rangle = 0$ for $i = 2, 3$. The cases simulated are summarized in Table 2. All the simulations were run for at least 10 eddy turnover times after transients. Throughout the text, we occasionally refer to cases with the Robin boundary condition as Robin-bounded and those with the no-slip condition as wall-bounded.

The motivation of using Eq. (4.1) is to provide a boundary for the flow that deviates from the behavior of a regular wall. Indeed, for large values of l, Eq. (4.1) constitutes a significant modification of the classic no-slip boundary condition by suppressing the formation of near-wall viscous layers (Lozano-Durán & Bae 2016). The mean tangential Reynolds stress is shown in Figure 5(a) for cases R550, R950, and R2000 with slip length $l = 0.10h$. For the three Reynolds numbers under consideration, $-\langle u_1 u_2 \rangle$ captures more than 90% of the total stress, and this was the criteria used to select $l = 0.10h$ as the reference slip length. As the Reynolds number increases, so does the contribution of $-\langle u_1 u_2 \rangle$ close to the wall at the expense of reducing the formation of near-wall viscous

Case	Re_τ	Δx_1^+	$\Delta x_{2,min/max}^+$	Δx_3^+	l/h	Driven by
R550	546	6.7	0.2/9.9	3.3	0.10	constant $\langle \frac{dp}{dx_1} \rangle$
R550-l1	546	6.7	0.2/9.9	3.3	0.25	constant $\langle \frac{dp}{dx_1} \rangle$
R550-l2	546	6.7	0.2/9.9	3.3	0.50	constant $\langle \frac{dp}{dx_1} \rangle$
R950	934	5.7	0.5/10.1	2.8	0.10	constant $\langle \frac{dp}{dx_1} \rangle$
R2000	2003	6.1	0.7/15.0	3.1	0.10	constant $\langle \frac{dp}{dx_1} \rangle$

TABLE 2. Tabulated list of cases. The numerical experiments are labeled following the convention R[Re_τ]-[specific case], where R denotes channel with Robin boundary condition. Δx_1, Δx_2 and Δx_3 are the streamwise, wall-normal and spanwise grid resolutions, respectively. The slip length is l. The last column shows the method employed to drive the channel flow. See text for details.

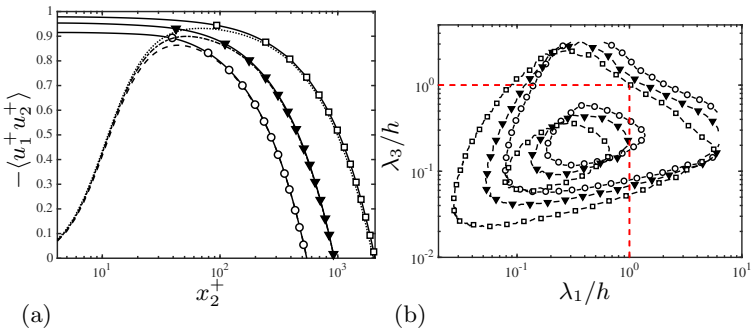

FIGURE 5. (a) Mean tangential Reynolds stress as a function of the wall-normal coordinate. Symbols are for Robin-bounded channels, ○, R550; ▼, R950; □, R2000. Dashed, dash-dotted, and dotted lines are for wall-bounded channels NS550, NS950 and NS2000, respectively. (b) Premultiplied wall-normal velocity spectra for Robin-bounded channels at $x_2 = 0h$. Contours are 0.1 and 0.6 of the maximum. The straight dashed lines are $\lambda_1/h = 1$ and $\lambda_3/h = 1$. Symbols are as in (a).

layers that appear prior to the proximity of the wall. Cases R550-l1 and R550-l2 are for $l = 0.25h$ and $l = 0.50h$, respectively, and are intended to test the effect of increasing slip lengths.

Another two important properties of the Robin boundary condition are that (i) it allows for transpiration at all flow scales and (ii), it does not encode any specific information regarding the linear wall-normal scaling of the log-layer eddies. The spectral density of the wall-normal velocity, ϕ_{22}, evaluated at $x_2/h = 0$ for Robin-bounded cases is shown in Figure 5(b) as a function of the streamwise and spanwise wavelengths, λ_1 and λ_3, respectively. The spectra are non-zero at the boundary and peak at $\lambda_1 \approx 0.3h$ and $\lambda_3 \approx 0.10h$, with a non-negligible contribution from wavelengths up to λ_1 and λ_3 of $\mathcal{O}(h)$. Moreover, the spectral energies obtained by integrating ϕ_{22} at $x_2 = 0h$ are $\approx u_\tau^2$, that is of the same order as the values in the bulk flow. This implies that the Robin

boundary should alter the behavior of eddies with sizes up to $\mathcal{O}(h)$ if they are controlled by the distance to the wall as commonly hypothesized (Townsend 1976).

4.2. *One-point statistics and spectra*

The mean streamwise velocities for the Robin-bounded and wall-bounded channel flows are compared in Figure 6. In Figure 6(b), the mean profiles for Robin-bounded cases are vertically displaced to match the centerline velocity of the corresponding no-slip case. A first observation is that the shape of $\langle u_1 \rangle$ remains roughly identical for $x_2 \gtrsim 0.10h$, and the Robin boundary condition is mainly responsible for a reduction of the total mass flux. The shifts required to match the Robin-bounded cases to their no-slip counterpart were positive and equal to 6.4, 8.0, and 8.9 plus units for R550, R950, and R2000, respectively. Nonetheless, we do not emphasize these values as they can be trivially changed by either adding a constant uniform velocity to the right-hand side of the Robin boundary condition in Eq. (4.1) or by a Galilean transformation of the velocity field.

The observations from Figure 6 can be connected to the law of the wall (Prandtl 1925; Millikan 1938; Townsend 1976),

$$\langle u_1^+ \rangle = \frac{1}{\kappa} \log\left(x_2^+\right) + B + \Pi, \tag{4.3}$$

where κ and B are the von Kármán and intercept constants for no-slip walls, respectively, and Π is an additional velocity displacement. From the integrated mean streamwise momentum balance, the mean velocity profile can be written as

$$\langle u_1^+ \rangle = \underbrace{l \left\langle \left. \frac{\partial u_1^+}{\partial x_2^+} \right|_w \right\rangle}_{\sim \Pi} + \underbrace{x_2^+ \left(1 - \frac{x_2}{2h}\right) + \int_0^{x_2^+} \langle u_1^+ u_2^+ \rangle dx_2'^+}_{\sim 1/\kappa \log(x_2^+) + B}, \tag{4.4}$$

and it is reasonable to hypothesize that the Robin boundary condition acts as an effective drag with a major impact on Π, while $\langle u_1^+ u_2^+ \rangle$ controls the x_2-dependent component, $\sim 1/\kappa \log(x_2) + B$, linked to the wall-normal mixing of the flow. Note that this is not strictly the case, and some coupling is expected between all terms in Eq. (4.4).

The r.m.s. velocity fluctuations for the Robin-bounded and wall-bounded channels are shown in Figure 7(a–c). The most remarkable observation from Figure 7 is that the Robin-bounded fluctuating velocities match quantitatively their wall-bounded counterparts for $x_2 \gtrsim 0.10h$ despite the lack of impermeable walls. The presence of a significant non-zero u_2 in Robin-bounded cases is evidenced by the r.m.s. of u_2 at $x_2 = 0$ whose values are comparable to the r.m.s. in the bulk flow. The result is again an indication that the total contribution of the wall-attached and -detached eddies to the turbulence intensities is insensitive to the presence of impermeable walls.

The spectral densities of the three velocity fluctuations, ϕ_{11}, ϕ_{22}, and ϕ_{33}, are shown in Figure 8 as a function of the streamwise and spanwise wavelengths. Several wall-normal heights are considered for R2000 and NS2000. Unsurprisingly, the spectra for the Robin-bounded and wall-bounded cases differ significantly in the proximity of $x_2 = 0h$. For the Robin-bounded case, ϕ_{22} is non-zero at the boundary and peaks at $\lambda_1 \approx 0.3h$ and $\lambda_3 \approx 0.10h$, with a non-negligible contribution from wavelengths up to λ_1 and λ_3 of $\mathcal{O}(h)$. We can then estimate the flow scales that are expected to be affected by the transpiration of the boundary by assuming that the stress-carrying eddies follow $\lambda_1 \approx 1.5x_2$ and $\lambda_3 \approx x_2$ (Dong *et al.* 2017). If the boundary is perceived as permeable for scales up to $\mathcal{O}(h)$, then attached motions below $x_2 \approx 0.7h$ should adjust accordingly to accommodate

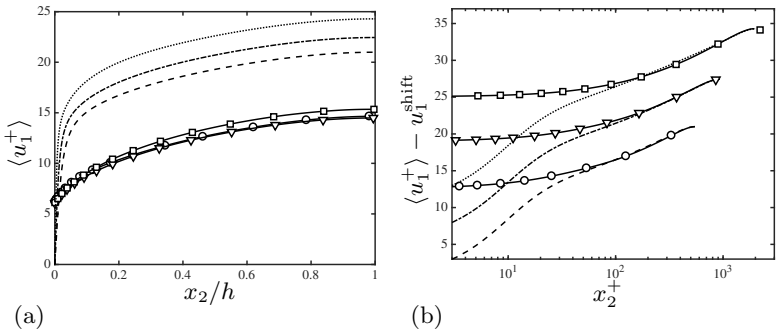

FIGURE 6. (a) Mean streamwise velocity profiles. (b) Mean streamwise velocity profiles with the centerline velocity of the Robin-bounded cases shifted to coincide with its corresponding wall-bounded case. Profiles at $Re_\tau \approx 950$ and $Re_\tau \approx 2000$ are additionally shifted by 5 and 10 plus units, respectively, for clarity. Symbols and lines are circles, R550; triangles, R950; squares, R2000; dashed line, NS550; dash-dotted line, NS950; dotted line, NS2000.

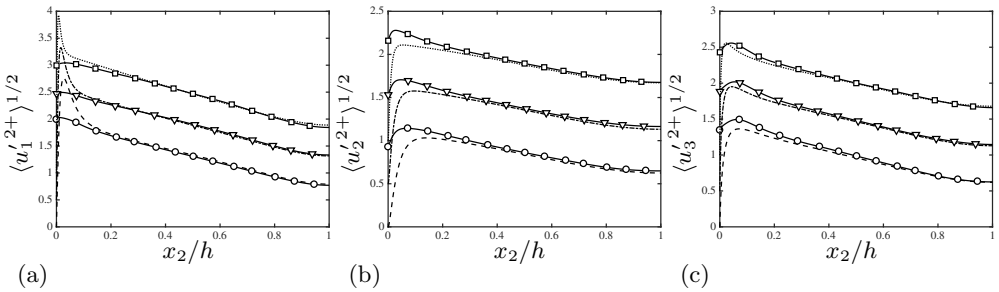

FIGURE 7. (a) Streamwise, (b) wall-normal, and (c) spanwise r.m.s. velocity fluctuations. Symbols and lines are: circles for R550, triangles for R950, squares for R2000, dashed line for NS550, dash-dotted line for NS950, and dotted line for NS2000. In all panels, the profiles for cases at $Re_\tau \approx 950$ and $Re_\tau \approx 2000$ are vertically shifted by 0.5 and 1 plus units, respectively, for clarity.

transpiration effects, especially if the wall is their primary organizing agent. However, inspection of the spectra above $x_2 \approx 0.10h$ shows that the agreement between wall-bounded and Robin-bounded channels is outstanding. Consequently, the distance to the boundary (or non-existent wall) is not the relevant length scale controlling the size of the attached eddies, in contrast with the traditional argument by Townsend (1976). Instead, the resemblance between wall-bounded and Robin-bounded cases presented above should be attributed to the common momentum transfer u_τ^2 characteristic of both cases as argued in Section 2.

4.3. *Logarithmic layer without inner-outer scale separation*

The Robin boundary condition imposes a new length scale to the eddies in the near-wall region. The characteristic flow length scales of the no-slip and Robin-bounded channels are plotted in Figure 9(a) as a function of x_2. The small, intermediate, and large scales are represented by the Kolmogorov length scale $\eta = (\nu^3/\varepsilon)^{1/4}$, the Taylor microscale

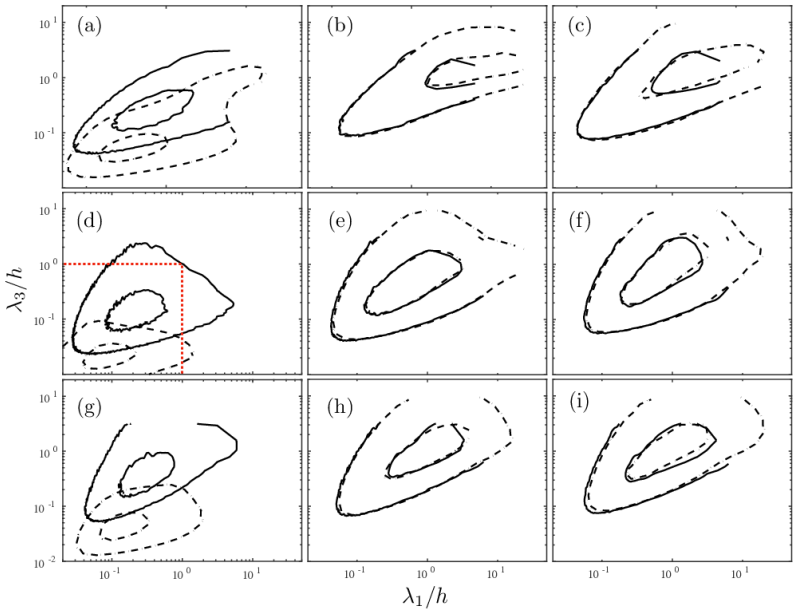

FIGURE 8. Wall-parallel premultiplied streamwise (a,b,c), wall-normal (d,e,f), and spanwise (g,h,i) velocity spectra at $x_2^+ = 0$ for R2000 and $x_2^+ = 1$ for NS2000 (a,d,g), $x_2^+ = 1001$ (b,e,h), and $x_2^+ = 2003$ (c,f,i). Solid lines are for the Robin-bounded channel (R2000) and dashed lines are for the wall-bounded channel (NS2000). Contours are 0.1 and 0.6 of the maximum. The red dotted lines are $\lambda_1 = h$ and $\lambda_3 = h$.

$\lambda_T = (15k/\varepsilon)^{1/2}$, and the integral length scale $L_\varepsilon = (k/3)^{3/2}/\varepsilon$, respectively, where ε is the rate of energy dissipation and k is the turbulent kinetic energy. Note that L_ε and λ_T drop rapidly to zero as x_2 approaches the wall for the no-slip channel, whereas they remain roughly constant in the Robin-bounded case. Moreover, the comparison of L_ε at two different Re_τ for the Robin-bounded channels shows that the integral length scale collapses in outer units across the entire boundary layer thickness, including the region close to $x_2 = 0h$. These results can be read as the disruption of the classic viscous scaling of the active energy-containing eddies at the wall, i.e., their sizes are a fixed fraction of h and do not decrease with Re_τ.

In spite of the lack of inner-outer layer scale separation with increasing Re_τ, the mean profile for Robin-bounded cases converges towards a log-layer at a similar rate as wall-bounded channels. This is shown in Figure 9(b) which contains the L_2-norm of the error function $\mathcal{E}_l = x_2^+ \partial\langle u_1^+\rangle/\partial x_2^+ - 1/\kappa$ with $\kappa = 0.384$ (Lee & Moser 2015) across $x_2 \in [0.1h, 0.2h]$ as a function of Re_τ. The outcome challenges the log-layer formulations derived from an inner-outer layer scale separation (Millikan 1938), since Robin-bounded cases approach a logarithmic profile as Re_τ increases despite the inner and outer length scale separation remains a constant fraction of h. Nonetheless, the Reynolds numbers in the present work are too low to attain a well-developed log-layer and, therefore, the results are indicative but not conclusive of the convergence of Robin-bounded cases to an actual wall-bounded log-layer as Re_τ increases.

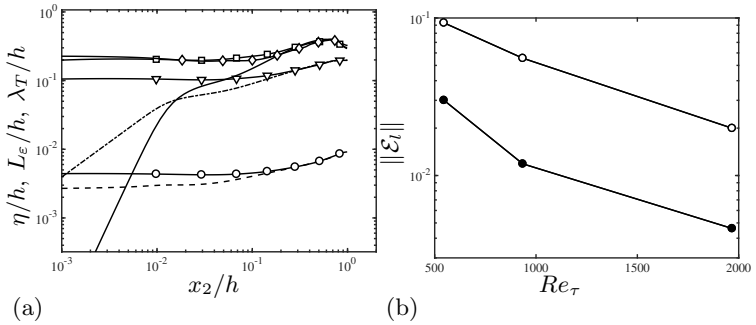

FIGURE 9. (a) Characteristic length scales. Kolmogorov length scale (NS550, dashed line; R550, circles), Taylor microscale (NS550, dot-dashed line; R550, triangles), and integral length scale (NS550, solid line; R550, squares; R950, diamonds). (b) L_2-norm of the error function $\mathcal{E}_l = x_2^+ \partial \langle u_1^+ \rangle / \partial x_2^+ - 1/\kappa$ with $\kappa = 0.384$ across $x_2 \in [0.1h 0.2h]$ as a function of Re_τ. Open and closed symbols are for wall-bounded and Robin-bounded cases, respectively.

5. Conclusions

In the present work we have proposed new characteristic velocity, length and time scales for the momentum-carrying eddies in the log-layer of wall-bounded turbulence. We have hypothesized that the mean tangential momentum flux and mean shear are the main contributors to the intensities, lifespan, and sizes of the active energy-containing motions in the outer region. The proposed characteristic scales are consistent with the predictions by Townsend's attached eddy model and extend its applicability to flows with different mean momentum flux. The mechanism proposed is as follows. The mean tangential momentum transfer defines a local-in-x_2 characteristic velocity scale u^*. The role of u^* is twofold: it controls the intensities of the active eddies and the mean shear. The size of the eddies is governed by the length scale l^* defined in terms of u^* and the characteristic time scaled t^* imposed by the mean shear. In this framework, the no-slip and impermeability constraints of the wall are not directly involved in the organization of the outer flow, and the role of the wall is relegated to serve as a proxy to sustain the mean momentum flux. The scaling proposed has been successfully assessed through a set of idealized numerical studies in channel flows with modified streamwise velocity profiles and mean pressure gradients.

We have further addressed the question of whether the impermeability of the wall is a foundational component of the outer-layer of wall turbulence by designing a new numerical experiment where the channel walls are replaced by a Robin boundary condition. In the resulting flow, instantaneous wall transpiration is allowed for scales comparable to the log-layer motions to the extent that the wall-normal distance can no longer be a relevant length scale. We have referred to this configuration as Robin-bounded channel flow as opposed to the traditional wall-bounded channel. A detailed inspection of the one-point statistics and spectra has shown that both wall-bounded and Robin-bounded channel flows share identical outer-layer motions, and we have interpreted this evidence as an indication that the same physical process occurs in both flow configurations.

Acknowledgments

This work was supported by NASA under Grant #NNX15AU93A. The authors thank Prof. Parviz Moin, Prof. Javier Jiménez, Dr. Perry Johnson, and Dr. Minjeong Cho for their insightful comments on previous versions of this manuscript.

REFERENCES

Adrian, R. J., Meinhart, C. D. & Tomkins, C. D. 2000 Vortex organization in the outer region of the turbulent boundary layer. *J. Fluid Mech.* **422**, 1–54.

del Álamo, J. C. & Jiménez, J. 2003 Spectra of the very large anisotropic scales in turbulent channels. *Phys. Fluids* **15**, L41–L44.

del Álamo, J. C., Jiménez, J., Zandonade, P. & Moser, R. D. 2004 Scaling of the energy spectra of turbulent channels. *J. Fluid Mech.* **500**, 135–144.

Bae, H. J., Lozano-Durán, A., Bose, S. T. & Moin, P. 2018*a* Dynamic wall model for the slip boundary condition in large-eddy simulation. *J. Fluid Mech.* pp. 400–432.

Bae, H. J., Lozano-Durán, A., Bose, S. T. & Moin, P. 2018*b* Turbulence intensities in large-eddy simulation of wall-bounded flows. *Phys. Rev. Fluids* **3**, 014610.

Bailey, S. C. C., Hultmark, M., Smits, A. J. & Schultz, M. P. 2008 Azimuthal structure of turbulence in high Reynolds number pipe flow. *J. Fluid Mech.* **615**, 121–138.

Bakken, O. M., Krogstad, P. Å., Ashrafian, A. & Andersson, H. I. 2005 Reynolds number effects in the outer layer of the turbulent flow in a channel with rough walls. *Phys. Fluids* **17**, 065101.

Bullock, K. J., Cooper, R. E. & Abernathy, F. H. 1978 Structural similarity in radial correlations and spectra of longitudinal velocity fluctuations in pipe flow. *J. Fluid Mech.* **88**, 585–608.

Chung, D., Monty, J. P. & Ooi, A. 2014 An idealised assessment of townsend's outer-layer similarity hypothesis for wall turbulence. *J. Fluid Mech.* **742**.

Davidson, P. A., Nickels, T. B. & Krogstad, P.-A. 2006 The logarithmic structure function law in wall-layer turbulence. *J. Fluid Mech.* **550**, 51–60.

De Graaff, D. B. & Eaton, J. K. 2000 Reynolds-number scaling of the flat-plate turbulent boundary layer. *J. Fluid Mech.* **422**, 319–346.

Dong, S., Lozano-Durán, A., Sekimoto, A. & Jiménez, J. 2017 Coherent structures in statistically stationary homogeneous shear turbulence. *J. Fluid Mech.* **816**, 167–208.

Flores, O. & Jiménez, J. 2006 Effect of wall-boundary disturbances on turbulent channel flows. *J. Fluid Mech.* **566**, 357–376.

Flores, O., Jiménez, J. & del Álamo, J. C. 2007 Vorticity organization in the outer layer of turbulent channels with disturbed walls. *J. Fluid Mech.* **591**, 145–154.

Guala, M., Hommema, S. E. & Adrian, R. J. 2006 Large-scale and very-large-scale motions in turbulent pipe flow. *J. Fluid Mech.* **554**, 521–542.

Hoyas, S. & Jiménez, J. 2006 Scaling of the velocity fluctuations in turbulent channels up to $Re_\tau = 2003$. *Phys. Fluids* **18**, 011702.

Hoyas, S. & Jiménez, J. 2008 Reynolds number effects on the Reynolds-stress budgets in turbulent channels. *Phys. Fluids* **20**, 101511.

Jiménez, J. 2004 Turbulent flows over rough walls. *Annu. Rev. Fluid Mech.* **36**, 173–196.

Kim, J. & Moin, P. 1985 Application of a fractional-step method to incompressible Navier-Stokes equations. *J. Comp. Phys.* **59**, 308–323.

Kim, K. & Adrian, R. J. 1999 Very large-scale motion in the outer layer. *Phys. Fluids* **11**, 417–422.

Lee, M. & Moser, R. D. 2015 Direct numerical simulation of turbulent channel flow up to $Re_\tau \approx 5200$. *J. Fluid Mech.* **774**, 395–415.

Lozano-Durán, A. & Bae, H. J. 2016 Turbulent channel with slip boundaries as a benchmark for subgrid-scale models in LES. *Annual Research Briefs, Center for Turbulence Research, Stanford University* pp. 97–103.

Lozano-Durán, A., Hack, M. J. P. & Moin, P. 2018 Modeling boundary-layer transition in direct and large-eddy simulations using parabolized stability equations. *Phys. Rev. Fluids* **3**, 023901.

Marusic, I. & Monty, J. P. 2019 Attached eddy model of wall turbulence. *Annu. Rev. Fluid Mech.* **51**, in press.

Marusic, I., Monty, J. P., Hultmark, M. & Smits, A. J. 2013 On the logarithmic region in wall turbulence. *J. Fluid Mech.* **716**, R3.

Meneveau, C. & Marusic, I. 2013 Generalized logarithmic law for high-order moments in turbulent boundary layers. *J. Fluid Mech.* **719**, R1.

Millikan, C. B. 1938 A critical discussion of turbulent flows in channels and circular tubes. In Hartog, J. P. D. & Peters, H. (Eds.) Proceedings 5th Int. Congr. Applied Mechanics. Wiley, pp. 386-392.

Mizuno, Y. & Jiménez, J. 2013 Wall turbulence without walls. *J. Fluid Mech.* **723**, 429–455.

Monty, J. P., Stewart, J. A., Williams, R. C. & Chong, M. S. 2007 Large-scale features in turbulent pipe and channel flows. *J. Fluid Mech.* **589**, 147–156.

Morrison, W. R. B. & Kronauer, R. E. 1969 Structural similarity for fully developed turbulence in smooth tubes. *J. Fluid Mech.* **39**, 117–141.

Orlandi, P. 2000 *Fluid Flow Phenomena: A Numerical Toolkit*. Springer.

Perry, A. E. & Abell, C. J. 1977 Asymptotic similarity of turbulence structures in smooth- and rough-walled pipes. *J. Fluid Mech.* **79**, 785–799.

Perry, A. E. & Chong, M. S. 1982 On the mechanism of wall turbulence. *J. Fluid Mech.* **119**, 173–217.

Prandtl, L. 1925 Bericht über die Entstehung der Turbulenz. *Z. Angew. Math. Mech.* **5**, 136–139.

Tomkins, C. D. & Adrian, R. J. 2003 Spanwise structure and scale growth in turbulent boundary layers. *J. Fluid Mech.* **490**, 37–74.

Townsend, A. A. 1976 *The Structure of Turbulent Shear Flow*. Cambridge University Press.

Tuerke, F. & Jiménez, J. 2013 Simulations of turbulent channels with prescribed velocity profiles. *J. Fluid Mech.* **723**, 587–603.

Vallikivi, M., Ganapathisubramani, B. & Smits, A. J. 2015 Spectral scaling in boundary layers and pipes at very high Reynolds numbers. *J. Fluid Mech.* **771**, 303–326.

Wray, A. A. 1990 Minimal-storage time advancement schemes for spectral methods. *Tech. Rep.* MS 202 A-1. NASA Ames Research Center.